

ENabling Optimized DISruptivE airframe-propulsion integration concepts

H2020 Research and Innovation Action
Grant Agreement No 860103

Deliverable Reference Number: D2.16

Deliverable Title:
WP2 Final Public Report

Lead participant: ONERA
Contributing participants: VKI, GPUP, TUD, ECL, UR3, DLR, UTWE, SISW

10 October 2023

Start date of project: 1st of June 2020
Duration: 48 months

APPROVAL

Title	Issue	Revision
WP2 Final Public Report	1	0
Author(s)	**Date**	
Eric Manoha (ONERA)	04/10/2023	
Approved by	**Date**	
Christophe Schram (VKI)	25/10/2023	

Contents

1 Introduction to ENODISE WP2 **5**

2 Noise source identification (Task 2.1) **5**
2.1 Context and objectives . . . 5
2.2 Involved partners and work distribution . . . 5
2.3 Main achievements . . . 6
2.4 Expected contribution in other project work packages . . . 7
2.5 Lessons learnt . . . 8
2.6 Deliverables . . . 8

3 Advanced data processing and management (Task 2.2) **8**
3.1 Context and objectives . . . 8
3.2 Involved partners and work distribution . . . 9
3.3 Main achievements . . . 9
3.4 Expected contribution in other project work packages . . . 10
3.5 Lessons learnt . . . 10
3.6 Deliverables . . . 11
3.7 Dissemination . . . 11

4 Low-order and semi-analytical methods (Task 2.3) **12**
4.1 Context and objectives . . . 12
4.2 Involved partners and work distribution . . . 12
4.3 Main achievements . . . 12
4.4 Expected contribution in other project work packages . . . 15
4.5 Lessons learnt . . . 16
4.6 Deliverables . . . 16
4.7 Dissemination . . . 16

5 High-fidelity CAA methods (Task 2.4) **17**
5.1 Context and objectives . . . 17
5.2 Involved partners and work distribution . . . 17
5.3 Main achievements . . . 17
5.4 Expected contribution in other project work packages . . . 19
5.5 Lessons learnt . . . 20
5.6 Deliverables . . . 20
5.7 Dissemination . . . 20

6 Optimization methods (Task 2.5) **20**
6.1 Context and objectives . . . 20
6.2 Involved partners and work distribution . . . 21
6.3 Main achievements . . . 21
6.4 Expected contribution in other project work packages . . . 23
6.5 Lessons learnt . . . 23
6.6 Deliverables . . . 23
6.7 Dissemination . . . 24

7 Propulsive efficiency and emissions (Task 2.6) 24
7.1 Context and objectives . . . 24
7.2 Involved partners and work distribution . . . 24
7.3 Main achievements . . . 24
7.4 Expected contribution in other project work packages . . . 25
7.5 Lessons learnt . . . 25
7.6 Deliverables . . . 26

8 Porous materials and advanced liners (Task 2.7) 27
8.1 Context and objectives . . . 27
8.2 Involved partners and work distribution . . . 27
8.3 Main achievements . . . 27
8.4 Expected contribution in other project work packages . . . 30
8.5 Lessons learnt . . . 30
8.6 Deliverables . . . 31
8.7 Dissemination . . . 31

9 Leading edge / trailing edge serrations (Task 2.8) 31
9.1 Context and objectives . . . 31
9.2 Involved partners and work distribution . . . 31
9.3 Main achievements . . . 31
9.4 Expected contribution in other project work packages . . . 33
9.5 Lessons learnt . . . 33
9.6 Deliverables . . . 33

10 Conclusions on WP2 33

1 Introduction to ENODISE WP2

ENODISE's architecture relies on four main pillars or WPs: WP3 (Experiments), WP4 (Simulations), WP5 (Optimization) and WP6 (Mitigation), the whole program relying on three families of experimental configurations A (DEP), B (BLI) and C (multi-rotors). In support of this structure, the objective of WP2 was to consolidate the background knowledge and methods of the partners, considering the specific challenges raised by the complex physical mechanisms and specific objectives of the project. As shown in Figure 1, WP2 contains 8 tasks aiming at the consolidation of knowledge and methods in the four pillars. The consolidation of the experimental (Tasks 2.1 and 2.2) and numerical methods (Tasks 2.3 and 2.4) were achieved in parallel with the design and realization of the experimental mock-ups, allowing to rapidly start the measurement campaigns of WP3 and the numerical activities of WP4. The optimization methods (Tasks 2.5 and 2.6) started later in view of the WP5 activities. Finally, the tools related to the design and manufacturing of the noise mitigation technologies (Tasks 2.7 and 2.8) have been operational for the start of the last pillar WP6.

ENODISE's WP2 involved 12 partners (out of 13) over 107 PM (out of 567) and produced 16 deliverables and the achievement of 8 milestones.

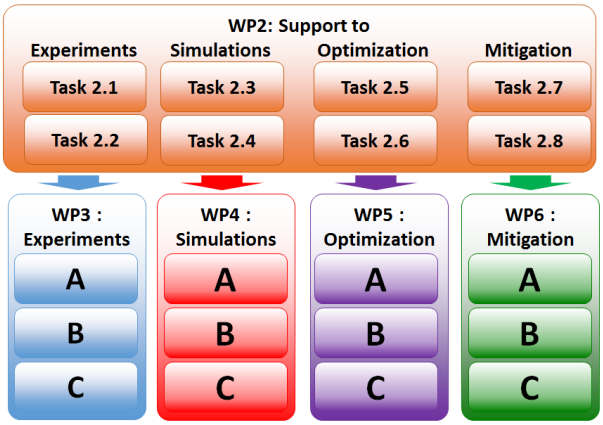


Figure 1: ENODISE structure and link of WP2's tasks to the four pillars.

The present report provides a synthesis of each task, including the context and objectives, the involved partners and work sharing, the main achievements, the expected contribution in other project work packages, and the lessons learnt. References of deliverables and related publications are also provided, with the possible dissemination actions expected in the future.

2 Noise source identification (Task 2.1)

2.1 Context and objectives

To improve beamforming analysis procedures: better spatial resolution and accurate quantification of sources, especially static and rotating sources lie in close proximity to each other.

2.2 Involved partners and work distribution

- TUD (Task leader): Beamforming method coupled with Phase-locked PIV-based surface pressure reconstruction
- VKI: Generalized Inverse Beamforming (GIBF) and Rotating Source Identification (ROSI)

2.3 Main achievements

VKI developed a dedicated acoustic beamforming technique for the identification and quantification of the various mechanisms, including turbulence interaction, flow non-uniformities, fluctuations in the trailing-edge boundary layer, and blade-tip leakages, which contribute to the sound produced by rotating blades. Precisely identifying these sound sources on the blade's surface is crucial for distinguishing and isolating these contributions and, consequently, for devising innovative noise reduction strategies. Deliverable 2.1 aims to introduce a cost-effective and efficient approach for isolating and quantifying noise-generating mechanisms on rotating blades using an irregularly shaped microphone array. The technique relies on the Rotating Source Identifier (ROSI) and was implemented and verified at VKI. To validate the method, simulated benchmark datasets involving rotating point sources emitting white noise were employed. The method's accuracy in localizing the sources and reconstructing their strength was assessed under both fixed and variable angular rates (figure 2). Furthermore, the algorithm's computational time, a primary limitation of ROSI, was mitigated through parallelization. Ultimately, this technique was applied to measure the noise sources produced by a forward-skewed subsonic axial fan operating at maximum efficiency. Successfully localizing and characterizing the principal noise sources on the blades was achieved in this instance.

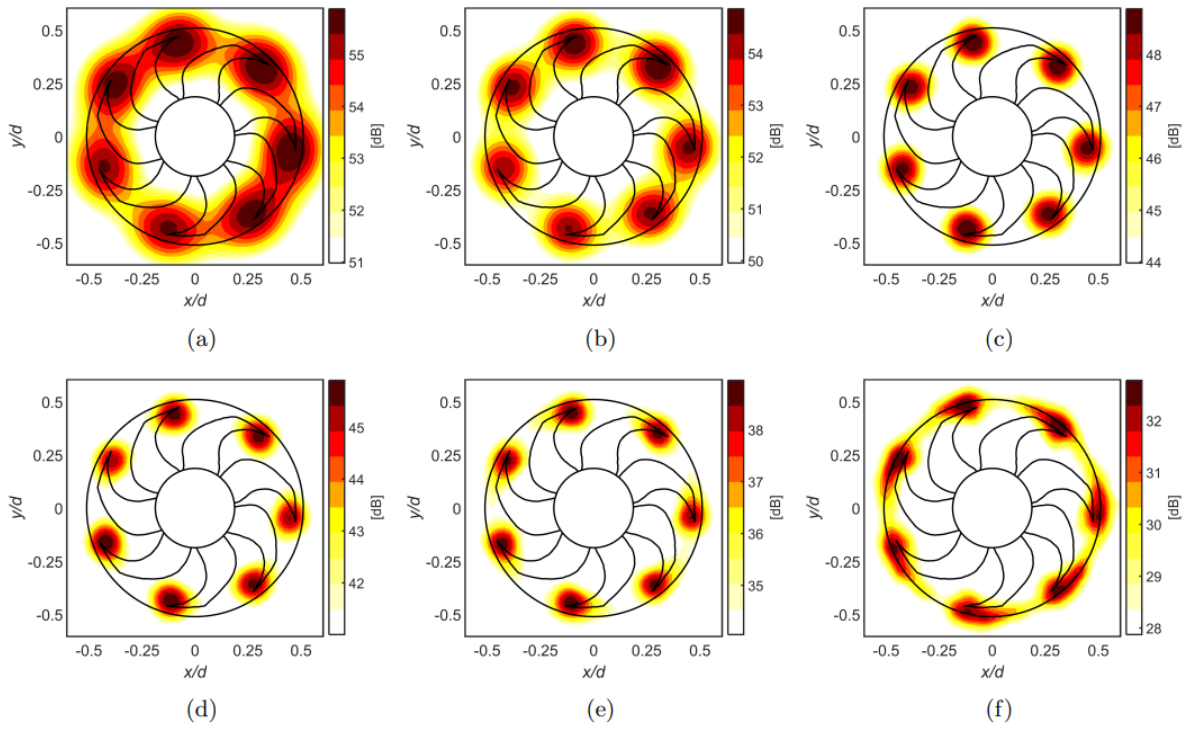


Figure 2: ROSI sound maps of the low-speed cooling fan referred to (a) $f_{1/3} = 3.15\,\text{kHz}$, (b) $f_{1/3} = 4\,\text{kHz}$, (c) $f_{1/3} = 5\,\text{kHz}$, (d) $f_{1/3} = 6.3\,\text{kHz}$, (e) $f_{1/3} = 8\,\text{kHz}$ and (f) $f_{1/3} = 10\,\text{kHz}$.

TUD developed a non-intrusive optical measurement technique that uses beamforming coupled with phase-locked PIV-based surface pressure reconstruction to improve noise source identification. TUD proposed this technique to accurately quantify fluctuating quantities in the flow field and connect them to the measured acoustic field. This method allows precise quantification of fluctuating amounts in the flow field without introducing new sources of perturbation. This technique helps to quantify the aerodynamic interferences emerging in the system, presumably due to installation effects. The data obtained by PIV can retrieve the pressure gradient and flow pressure in 2D and 3D configurations. In propeller applications, the pressure field can be extracted around the blade and in the propeller slipstream to obtain aerodynamic

data and connect it to the installation effects without adding new perturbations to the system. Therefore, in a Distributed Propeller (DP) setup, the proposed technique offers a non-intrusive method of collecting data that can help researchers better understand the aerodynamic interferences and their impact on the noise generated by such a system. This breakthrough could lead to a further understanding of the aerodynamics and acoustics of DP aircraft, resulting in more efficient and quieter designs.

The technique described in a previous study [1] was applied to the flow field at the tip of a transonic propeller blade. A stereoscopic PIV flow investigation was performed, merging seven cross-sectional measurement planes near the blade tip. The pressure field was calculated using assumptions such as adiabatic flow and quasi-steady flow. It was computed using the PIV data and integrating the governing equations in the compressible regime. The resulting data was compared to a numerical RANS-periodical steady computation of the propeller model, with maximum differences of about 10%. The original publication [1] provides further analysis details, including an overview of the propeller and the positioning of the measurement planes, as illustrated in Figure 3.

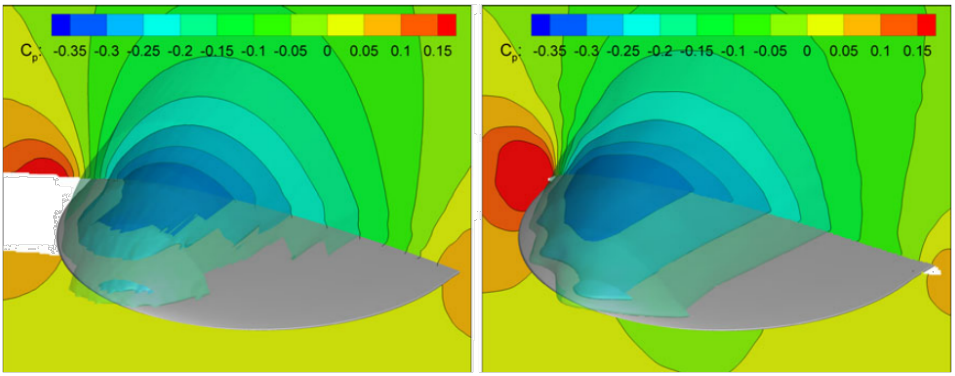


Figure 3: Comparison between PIV integrated pressure coefficient (left) and RANS computed pressure coefficient (right) [1].

The volumetric flow field required for the pressure reconstruction can also be obtained using 3D Particle Tracking Velocimetry (3D-PTV) techniques, such as the widely applied "Shake-the-box"[2]. Here, discrete positions of the particles along their trajectory are fitted by a polynomial function. This function regularizes the particles' position, velocity and acceleration. Consequently, information on the acceleration and velocity of the flow is returned at scattered locations through the measurement domain. The benefits of the 3D-PTV algorithms are the higher computational efficiency and local accuracy compared to a standard tomographic reconstruction [2].

Lagrangian Particle Tracking techniques allow for time-resolved volumetric flow measurements from which the pressure can be reconstructed. The tracks are typically transported to a cartesian technique by Gaussian Binning. Since the allowable seeding density is typically low, this limits the spatial resolution of the results and therefore small flow structures cannot be resolved. A fine scale reconstruction method name VIC+ [3] is proposed to resolve this issue. In VIC+ the velocity material derivative is used to increase the spatial resolution. The technique has been successfully applied to the wake of an isolated rotor in Figure 4.

2.4 Expected contribution in other project work packages

VKI The beamforming techniques are intended to be used for the measurement of the single and coaxial propeller noise (configuration C) to be investigated in WP3.

TUD The proposed experimental technique aims to obtain aerodynamic data for Configuration B1 of the ENODISE project during Work Package 3. The technique is a solution for assessing aerodynamic interferences occurring in DP setups, such as the one presented in Configuration B1. Since the propulsion system is tightly integrated with the airframe in this setup, it generates a complex flow field with many

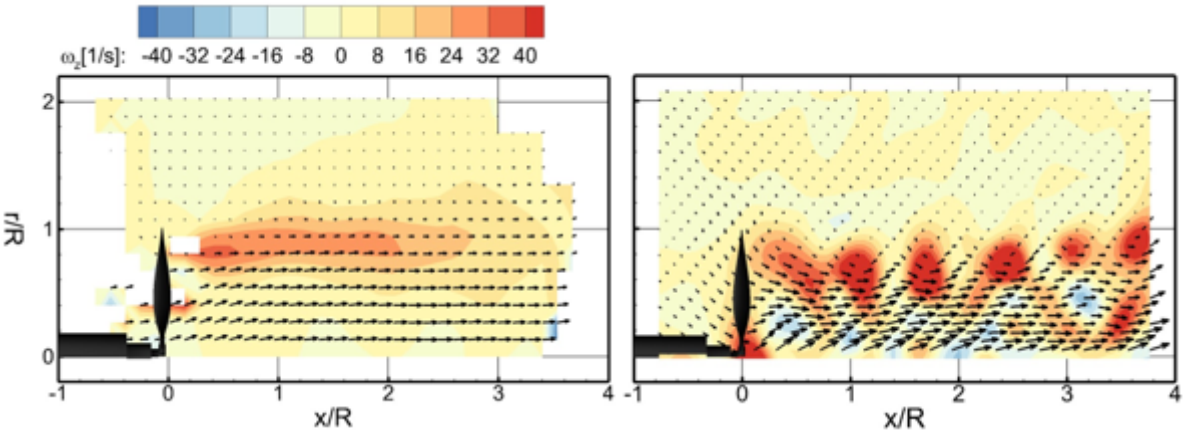


Figure 4: Reconstructed instantaneous out-of-plane vorticity field ωz and 2D velocity vectors of a single isolated small scale propeller, reconstructed using Gaussian Binning (left) and VIC+ (right).

components. This technique is useful because it avoids intrusive measurement techniques that could impact the acquired data, which is difficult to access in DP setups.

2.5 Lessons learnt

VKI In this task, we learned that utilizing an irregularly shaped microphone array with the ROSI technique offers a cost-effective and efficient means of pinpointing and quantifying noise sources on rotating blades. Nevertheless, applying this technique to drones and UAVs, where tonal noise is crucial and multiple rotors may operate at varying RPMs, introduces additional complexities that demand further research and adaptation to effectively address these specific challenges in drone noise characterization and mitigation.

TUD Additionally, the beamforming method coupled with Phase-locked PIV proposed in this document provides a non-intrusive method for collecting aerodynamic data in DP setups, allowing for a better understanding of the aerodynamic interferences and their impact on noise generation. By using VIC+, it is possible to reconstruct the time-resolved 3D slipstream characteristics of propellers from sparsely seeded velocimetry data. The reconstructed data can be used as an input for the pressure reconstruction to identify potential noise sources.

2.6 Deliverables

D2.1 - Improved GIBF and ROSI algorithms - A. Zarri (VKI), R. Zamponi (VKI), September 6, 2021.

D2.2 - Beamforming method coupled with phase-locked PIV-based surface pressure-reconstruction algorithm - D. Ragni (TUD), F. Monteiro (TUD), H. Dekker (TUD), September 21, 2021.

3 Advanced data processing and management (Task 2.2)

3.1 Context and objectives

During ENODISE, extensive experimental campaigns performing parametric studies are performed, along with a number of numerical simulations. This produces a large amount of data that needs a management plan to ensure its usability in the future as well. The task also explored methodologies for extracting

information from large amounts of data, with specific application to pressure data obtained both numerically and experimentally. Advanced post-processing techniques based on wavelet transform and Proper Orthogonal Decomposition (POD) have been developed and assessed to educe coherent structures embedded in the flow with the aim of getting a physical insight into the rotor noise generation mechanism. Several data mining techniques have been identified as useful strategies for interpolation and modelling, the effectiveness and usability of which depend on the problem dimension and on the data distribution within the domain.

3.2 Involved partners and work distribution

- UR3 (Task Leader): POD and wavelet methods for the extraction of hydrodynamic and acoustic installation effects
- UR3/VKI: Data mining methods for large experimental and numerical datasets based on the JASON format and a specific indexation system

3.3 Main achievements

In Deliverable 2.4, a data management plan was redacted. The task identified the use of space-, comma- or tab- separated data files to store large lookup tables collecting the results of simulations and/or experiments. In addition, the JSON format has been identified as an extremely lightweight and understandable text format for data interchange, that takes advantage of a wide set of open-source tools and API for file management in almost all high- and low-level programming languages. For the same reason, Hierarchical Data Format in the newer HDF5 format is identified for creating containers of data with complex relationships and dependencies (multidimensional lookup tables, groups of datasets, etc.). In order to guarantee the re-usability of data, it is fundamental to add documentation for them. Any directory containing data is required to be joined with a README.txt file containing tailored information. POD techniques previously used to detect coherent structures embedded in turbulent jets have been tested and applied to rotor configurations. Wavelet-based techniques providing the decomposition of the hydrodynamic and acoustic pressure signatures and conditioned statistics have been tested and validated on an experimental database provided by TuDelft. An innovative wavelet-based separation procedure of the tonal and broadband components of a rotor noise spectrum (Figure 5) has been developed ad hoc and successfully applied to an experimental database of a low Reynolds-number single propeller, provided by TuDelft. The technique achieves the decomposition of the tonal and broadband components as time series, which represents the main advancement with respect to existing methodologies.

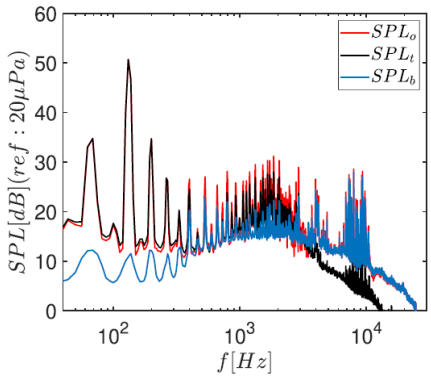


Figure 5: An example of separated spectra.

Regarding the data mining task, several data mining techniques were identified as useful strategies for interpolation and modelling, the effectiveness and usability of which depending on the problem dimension and on the data distribution within the domain. B-spline interpolation (Figure 6) of various order are

commonly used techniques for data arranged in structured grids; nearest neighbour interpolation (Figure 7) and inverse-distance weighting (Figure 8) can be effectively used with multivariate interpolation of scattered data; the active Artificial Neural Network metamodelling (Figure 9) developed by UR3 allows to build an analytic function, automatically selecting the network topology and activation functions, and providing also an estimate on the prediction accuracy where the true values are unknown.

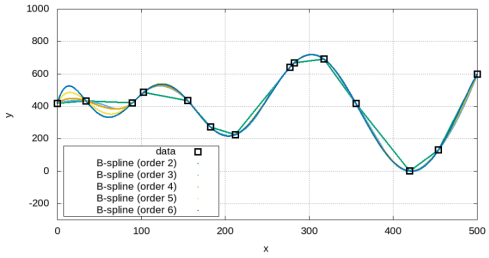


Figure 6: B-Spline interpolation of various orders of a test function.

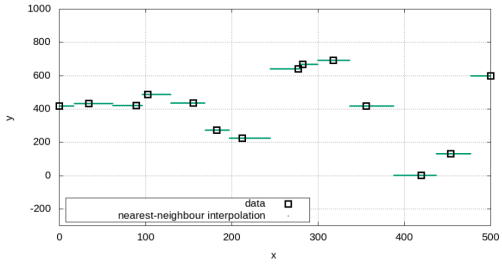


Figure 7: Nearest neighbor interpolation of a test function.

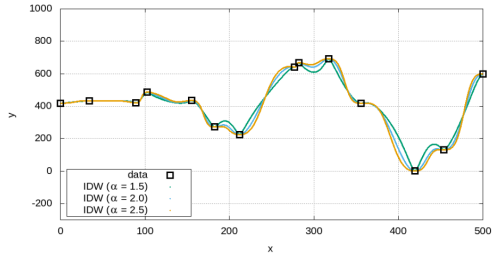


Figure 8: Inverse Distance Weighting interpolation of a test function.

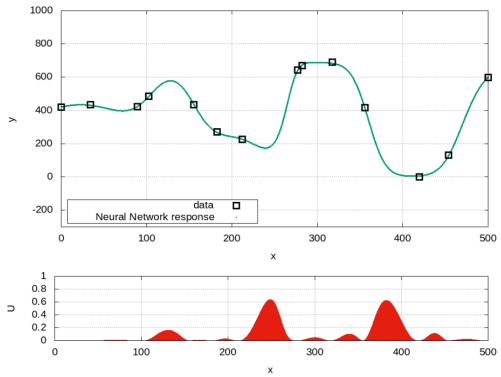


Figure 9: Artificial Neural Network prediction with uncertainty of a test function.

This last feature plays a key role. Indeed, the fitting capabilities on the training set do not give any information about the metamodel behaviour in the rest of the domain. The global uncertainty can successfully drive the designer towards the selection of new points where perform additional experiments.

3.4 Expected contribution in other project work packages

The application of the above-mentioned POD and wavelet-based techniques to experimental and numerical databases would be a pertinent approach to explore the physical mechanisms of rotor noise in both isolated and installed configurations. Specifically, the coherent structures most efficient for noise emissions can be identified, characterised and foundations for their modelling could be potentially laid.

The data mining techniques described above will constitute the basis for the metamodeling of experimental and numerical data produced in WP3 and numerical simulation data produced in WP4. The resulting metamodels will be fundamental for the the robust/reliability based optimization framework developed by UR3 that will be applied to the selected configuration in WP5.

3.5 Lessons learnt

Regarding the application of advanced data processing techniques, the analysis of the separated tonal and broadband components provides a clear picture of the different source behaviour of rotor noise.

Specifically, the tonal directivity of a single propeller shows a dipole-like shape and it is weakly affected by the advance ratio, unlike its amplitude. The broadband component directivity is mainly directed towards the wake region downstream of the propeller, most likely as an effect of the blade vortex noise (see Figure 10). We note that these features could not be inferred by the analysis of the original signals. Metamodels are demonstrating to be suitable to modern approaches to the noise–constrained design in aeronautics, and the recent availability of wide computing resources brought to a massive use of Artificial Neural Networks (ANN) in the surrogate modelling process. The set of topologies capable to correctly fit the training data is strongly problem dependent and there is not a specific scheme to find the optimal or near–optimal number of hidden layers and nodes. The active approach developed by UR3 is used to automatically select the architecture that ensures the desired fitting accuracy. Techniques such as the update of the learning rate, the use of an early stopping criterion, the automatic selection of activation functions and the optimization of the network topology demonstrated to be fundamental features for a fast and reliable creation of the network, mitigating the effect of instabilities in the training and foreseeing the fitting capability of a network and decide whether change architecture during the training.

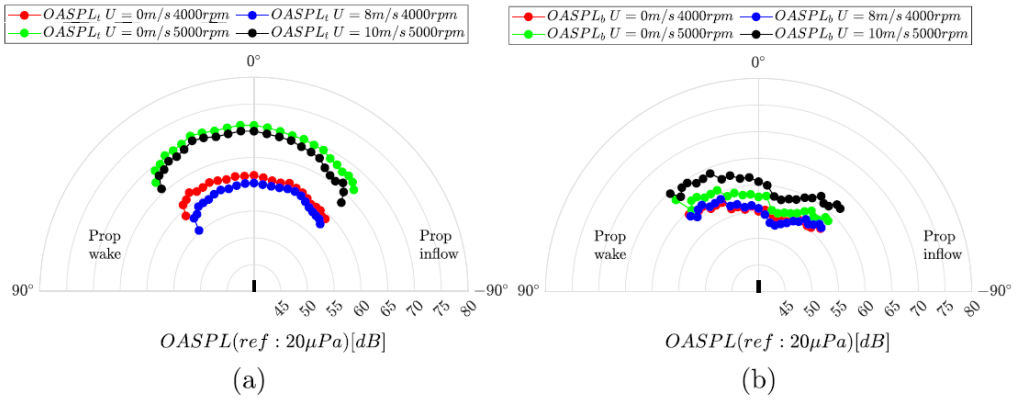


Figure 10: OASPL directivities. a) tonal component; (b) broadband component.

3.6 Deliverables

D2.3 - POD and wavelet methods for the extraction of hydrodynamic and acoustic installation effects - Roberto Camussi and Stefano Meloni (UR3) - 21 September 2021

D2.4 - Data mining methods for large experimental and numerical datasets - Francesco Centracchio (UR3) - 6 September 2021

3.7 Dissemination

S. Meloni, E. de Paola, E. Grande, D. Ragni, L.G. Stoica, A. Di Marco and R. Camussi, Wavelet-based decomposition of the tonal-broadband components of propeller noise, AIAA 2022-2876.

Meloni S., De Paola E., Grande E., Ragni D., Stoica L.G., Di Marco A., Camussi R.,"A wavelet-based separation method for tonal and broadband components of low Reynolds-number propeller noise", Measurement Science and Technology Vol. 34, 044007, 2023.

Meloni S., De Paola E., Centracchio F., Iemma U., Camussi R., "Experimental characterization and data-driven modelling of unsteady wall pressure fields induced by a supersonic jet over a tangential flat plate", Journal of Fluid Mechanics, Vol. 958, A93, 2023.

4 Low-order and semi-analytical methods (Task 2.3)

4.1 Context and objectives

To improve low-order and semi-analytical methods to account for complex installation effects.

4.2 Involved partners and work distribution

- ECL : extension of two advanced analytical models developed for DEP systems, one for loading-noise sources, one for scattering by a truncated half-plane
- VKI (Task Leader): extension of BATMAN solver to account for potential flow distortion (wing leading edge/puller propeller)
- SISW: coupling BATMAN with BEM/FEM solvers (SimCenter 3D) for acoustic shielding effects
- NLR: adapt an existing/validated analytical method for propeller noise prediction to account for non-uniform flow
- ONERA: coupling sound synthesis tools with the low-order models

4.3 Main achievements

ECL/VKI/SISW A global analytical prediction scheme of propeller tonal noise was developed, from source and scattering models available at ECL. It is dedicated to typical wing-propeller arrangements corresponding to configuration B2, involving two side-by-side propellers installed in the rear part of a wing. The modeling approach is in two steps. In the first step, the blade forces acting as equivalent dipole sources are determined. Steady forces are inferred from the blade-element momentum theory and/or from computations by partners. Lift fluctuations responsible for unsteady-loading noise are determined by Sears' or Amiet's theory, from stationary velocity distortions assumed known (again, either provided by partners or estimated with ad-hoc models). Equivalent circular arrays of stationary phased dipoles called source-modes are introduced. In a second step, the radiation of source-modes is calculated at any point, including sound scattering by the wing, *via* the use of an appropriate Green's function. The latter is a modified version of the half-plane Green's function, assimilating the wing to a rectangular plate of finite chords. Outputs of the model are tonal noise levels and associated three-dimensional directivity diagrams. Despite its simplifications, the model allows to quantify sound masking and diffraction effects by the wing. Repeated calculations within the scope of optimization algorithms are possible at a reasonable cost. Typical simulated sound fields are shown in Fig. 11, illustrating the crucial effect of propeller positioning.

In Task 2.3, **VKI** and **SISW** collaborated in order to improve the numerical efficiency of the coupling between semi-analytical and numerical acoustic solvers. In order to efficiently account for scattering surfaces in the numerical simulations, Amiet's analytical models for leading and trailing edge broadband noise implemented in BATMAN$^{\pi}$ solver have been successfully coupled with tailored Green's functions (also called Acoustic Transfer Vector (ATV) technology) computed from Finite Element Method (FEM) or Boundary Element Method (BEM) available in SISW commercial acoustic solver Simcenter 3D. The validity of this FEM/BEM-ATV coupling has been verified for a simplified scattering plate-airfoil test case for which an analytical solution is available using an image source approach. The test case consisted in computing the noise radiated from the trailing-edge noise of an infinitely thin airfoil in a flow at a velocity of 16 m/s in the presence of an infinite flat plate parallel to the airfoil chord-span plane. The results obtained using the BEM-ATV and FEM-ATV methods closely reproduced the acoustic directivity and amplitude obtained with the image source model used as a reference. In order to improve the numerical efficiency of this coupling, dedicated methods have also been developed in the context of ENODISE namely:

- Derivation of an ATV formulation based on a high-order FEM adaptive order approach, named FEMAO. FEMAO has shown to provide superior performance on a wide variety of Helmholtz problems compared to conventional FEM models. This FEMAO-ATV feature has been released in Simcenter 3D Acoustics.
- Derivation of FEMAO-based ATV formulation for arbitrary mean flow for improved numerical accuracy for flow acoustics problems.
- Derivation of a fast wavenumber integration approach to reduce the computational cost of the coupling between semi-analytical and numerical acoustic solvers.
- Improvement of the computational efficiency of Simcenter 3D FEM solver for acoustic simulations, including a better management of both the memory (RAM), the FEM element orders and the propeller noise sources.

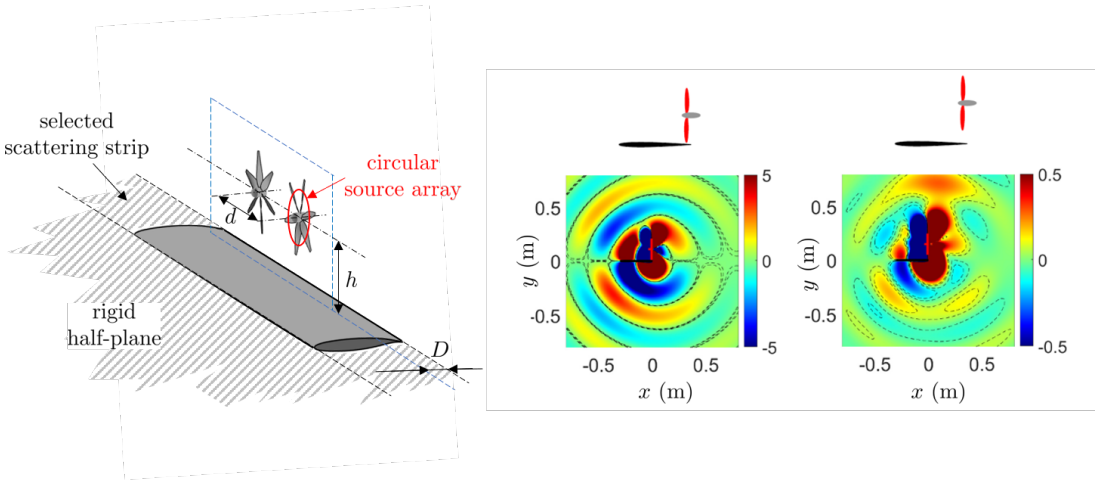


Figure 11: Left: main positioning parameters of configuration B2, definition of the scattering strip mimicking the wing. Right: instantaneous sound-pressure maps, side view, wing section and propeller disc featured by black and red segments.

NLR 's contribution to the development of low-fidelity methods consisted of two parts, to be applied to configuration B (multiple propellers on top of a wing):

- Consolidation of a lifting-line method for the tonal noise of a propeller in a non-uniform flow.
- Development of a simplified Boundary Element Method to account for the scattering by a wing.

NLR uses a lifting-line approach that is based on the method of matched asymptotic expansions, applied to a set of rotating straight blades. It consists of both an aerodynamic part and an acoustic part. The aerodynamic part provides solutions for the steady aerodynamic flow field and the lift distribution along the blades, assuming a uniform flow in the direction of the propeller axis. The lift distribution is used as input for the acoustic computation. If the flow is not uniform, the lifting-line model needs to be extended. This is done by assuming that the flow perturbations cause a small linear fluctuation of the forces on the propeller blades. To account for a finite response time the Sears function is applied. To account for the presence of a wing, a Boundary Element Method (BEM) is applied. This method is only valid if the scattering surface is smooth, which is not the case if the wing has a sharp trailing edge. It is assumed that if this edge is replaced by a rounded edge, with a dimension much smaller than the wavelengths of interest, the error in the computation will be small. If a full 3D BEM is applied, the method turns out to be computationally demanding. The system of equations can be solved either by

matrix inversion or iteration. In the first case the memory requirement exceeds that of a standard PC. In the case of an iterative solution, it is difficult and time-consuming to achieve a converged solution. Therefore, the wing is replaced by an infinitely long cylinder with a representative cross-section. This allows the application of a Fourier transform in spanwise direction. For each Fourier mode a 2D BEM equation is found that can be solved easily by matrix inversion. For the application in task 4.2 both the lifting-line and BEM methods are used in conjunction with a RANS method applied to an actuator disc above the wing (see Figure 12). Some results for the propeller-wing configuration as tested by NLR are given in Figures 13 and 14.

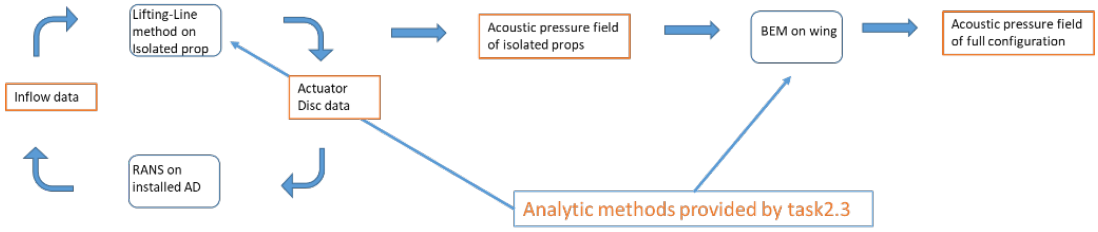


Figure 12: NLR's chain of computations to be used in task T4.2

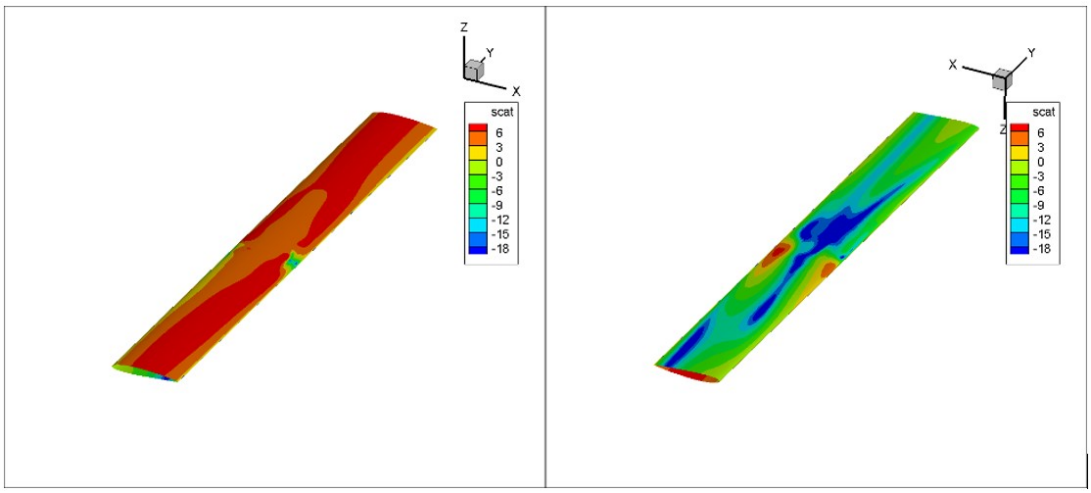


Figure 13: Scattering effect (in dB, BPF) on the surface of the wing. Left: Upper side. Right : lower side

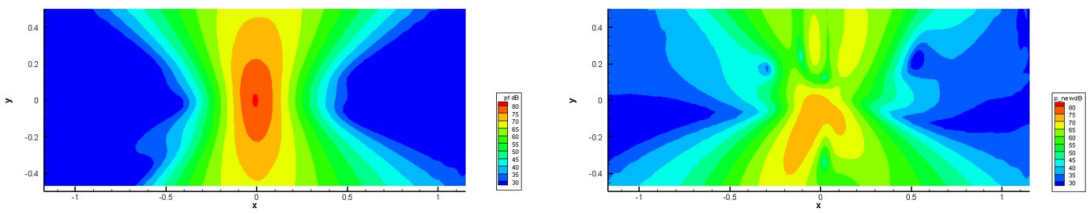


Figure 14: Noise levels on a surface below the wing. Left : Without wing. Right : With wing

ONERA In the context of ENODISE, a lot of effort is put into measuring and predicting absolute noise levels from different airframe-propulsion systems, including installation effects. In the era of perception-based aircraft design, human perception of the emitted noise becomes a new driver, besides the usual

assessment methodologies using metrics based on pure physics. In ENODISE, ONERA's task is to implement a fast simulation chain aimed at reproducing the essential perceptive features associated with novel disruptive integrated propulsive concepts. To that end, the output of the low-order models developed in WP2 is coupled with a sound synthesis tool, making the noise emission audible. In WP2, the adequacy of the existing noise synthesis tool FLAURA [4] to deal with the specific ENODISE configurations is considered. FLAURA, for "FLyover AURAlization", is an ONERA in-house noise synthesis tool for the generation of audible sounds from numerical data. It has been developed as a complementary module to the System Noise Prediction Tool CARMEN [5] [6]. Two versions of the tool are available, FLAURA-F and FLAURA-T, assuming a propagation in the, respectively, frequency and temporal domains. As illustrated by Figure 15, FLAURA-F starts from noise spectra generated at the receiver position, including installation and propagation effects, then tonal and broadband components are separated before an inversed Fourier transform (IFT) provides temporal signals. On the other hand, in FLAURA-T the switch from frequency to temporal domain (via IFT) happens at source level and acoustic waves are propagated to the ground in the temporal domain, keeping the phase information, accounting for all atmospheric propagation effects. Both tools typically consider a moving source and a fixed observer, so simplified versions will be used in ENODISE experiments, where the source and the observer are fixed. The question of which version of the tool should be used in WP 4 depends on the propagation effects to be considered, and on the exact nature of the data that will be available. In WP2 the method is applied to a simple single propeller case for which the PSD is independent of the phase information, and is therefore identical for both approaches. For multi-propeller configurations FLAURA-T will be used to prescribe phase shifts between propellers.

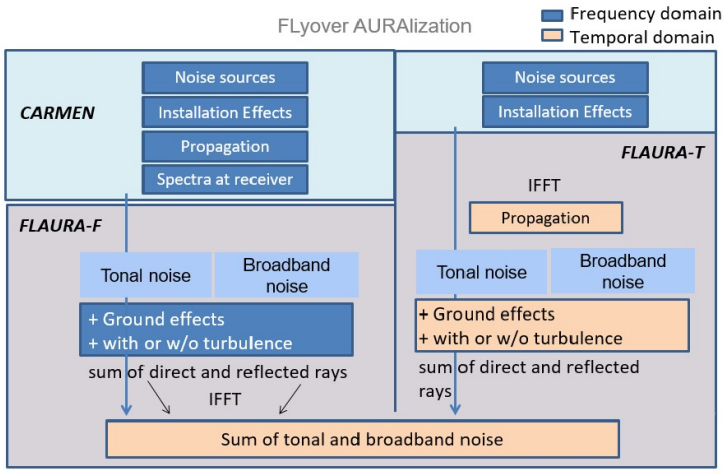


Figure 15: CARMEN-FLAURA chain structure

4.4 Expected contribution in other project work packages

ECL/VKI/SISW The analytical models are applicable to true parameters of the experiment in configuration B2. The measurements are part of WP3 and the application for the determination of optimal sets of parameters is part of WP4. Comparison of measured and predicted tonal-noise spectra contributes to validating the models. Then the latter helps to understand the dominant underlying physical mechanisms.

NLR The low-fidelity methods developed by NLR in task 2.3 have been applied in task 4.2, in conjunction with a RANS computation. The application is the propeller on top of a wing configuration, as tested in the acoustic wind tunnel AWT of NLR.

ONERA The fidelity of the sound synthesis will be assessed by comparing the spectrograms measured in WP3.2 and simulated in WP4 using the WP2 low-order models on one hand, and through unofficial, rapid listening sessions on the other. As a by-product, if they are deemed realistic, the auralizations will serve for communication purposes.

4.5 Lessons learnt

ECL/VKI/SISW Analytical predictions of sound scattering of propeller noise by the trailing edge of a wing, in typical B2 configurations, highlighted a regime of amplification of the tonal noise when blade tips operate at acoustically-compact distance from the edge. This effect can be avoided by proper design. Analytical modeling can be achieved with only an approximate and incomplete description of the addressed system, at the early design stage.

The work carried out in the context of the coupling between semi-analytical and numerical acoustic solvers highlighted the benefits of using the high-order adaptive FEM approach FEMAO for the ATV computation in terms of computational cost and storage, especially in the context of large-scale engineering problems arising in acoustics.

NLR The application of a BEM method to a full 3D configuration turned out to be rather difficult and cumbersome, given the limited resources and time. However, allowing a simplification of the method, specific for the configuration of interest, a fast and robust method has been developed. The results look plausible.

ONERA The auralization tool developed by ONERA, FLAURA, is adapted to most ENODISE configurations. In WP2 it was applied to a single propeller case. More investigation will be required when multi-propeller data and low-order noise models become available in WP4.

4.6 Deliverables

D2.5 - Upgraded and computationally-efficient semi-analytical models and coupling with FEM/BEM solvers - J. Christophe (VKI), M. Roger (ECL), H. Beriot (SISW), M. Tuinstra (NLR) - April 30, 2022

D2.7 - Low-order model-based sound synthesis method for the assessment of airframe-propulsion installation effects - I. LeGriffon (ONERA) - G. Bampanis - 27 January 2022

4.7 Dissemination

H.N.J. Dekker, H.H. Brouwer, J.C. Kok, M. Laban and M. Tuinstra, 'Tonal noise measurements and simulations of an Over-The-Wing propeller', AIAA 2023-3358.

Roger M., Acevedo Giraldo D. & Jacob M., Acoustic versus aerodynamic installation effects on a generic propeller-driven flying architecture, *Int. J. of Aeroacoustics*, **21**(5-7), pp. 585-609, 2022.

Acevedo Giraldo D., Roger M., Jacob M. & Bériot H., Analytical study of the aerodynamic noise emitted by distributed electric propulsion systems, *28th AIAA/CEAS Aeroacoustics Conference*, paper 2022-2830, Southampton, 2022.

Le Bras S., Gabard G., & Bériot H., Direct and adjoint problems for sound propagation in non-uniform flows with lined and vibrating surfaces, *Journal of Fluid Mechanics*, **953**, A16, 2022.

5 High-fidelity CAA methods (Task 2.4)

5.1 Context and objectives

To improve high-order methods to account for complex installation effects and provide validation data sets.

5.2 Involved partners and work distribution

- DLR (Task leader): Fast broadband noise prediction from inflow turbulence: RANS mean flow (propeller = actuator disk) then FRPM adapted to turbulence anisotropy
- GPUP: CABARET solver for hi-fi CAA, based on WMLES, compatible with OpenFOAM, FW-H solver (GPU)
- ONERA: adaptation of ZDES mode #3 to the additional use of wall models coarser near-wall grid resolution
- RWTH: Generalized model for arbitrary distribution of porous materials (Brinkman) in coupled CFD/CAA solver

5.3 Main achievements

ONERA developed a numerical method based on the coupling between the WMLES mode of ZDES (mode 3) and a wall model in a Cartesian octree grids framework. It allows a direct resolution of the turbulent scales present in the outer region of boundary layers, while the use of a wall model in the inner region (resolved in RANS mode) gets rid of the usual grid requirement y+=1 near the wall and consider coarser grid resolutions (y+ 50) to save computational resources. The method was validated by the test case of the boundary layer developing over a flat plate (see Figures 16 and 17), with an inflow tripping strategy based on the local introduction of small vertical rods.

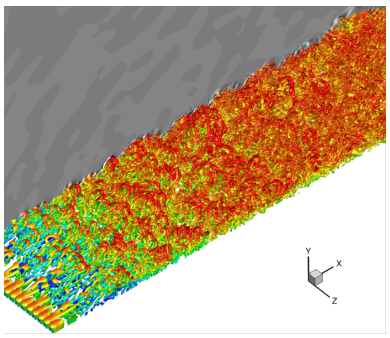


Figure 16: ZDES with wall law computation of the flat plate test case. Instantaneous visualization using iso-Q criterion surfaces.

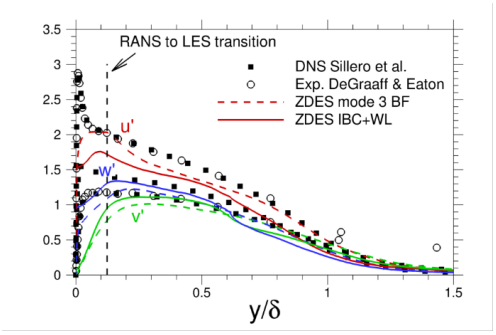


Figure 17: ZDES with wall law computation of the flat plate test case. Resolved velocity fluctuation profiles at $x/\delta = 45$, in wall units, compared to available experimental and numerical reference results.

DLR developed a non-empiric prediction workflow for propellers under general installation conditions utilizing a Computational Aeroacoustics (CAA) approach based on linear (specifically: linearized Euler (LEE) and linearized Navier-Stokes equations (LNS)) or non-linear perturbation equations (NLDE). The problem was split into a time-averaged flow part derived from steady-state RANS CFD simulation and

a subsequent unsteady acoustic simulation step. In the basic approach, an actuator-disk AD-RANS mean flow simulation wasd used to model the rotating propeller blades by means of regularized rotating displacement and momentum line sources on the fixed CAA grid. This way the resolution of the rotating propeller geometry was omitted and resolution requirements can be reduced to typically about 10 points over the blade chord. Sound propagation and, e.g. blade tip vortices and interaction noise stemming from interaction with downstream obstacles were resolved as part of the CAA simulation by means of low dispersive and dissipative models.

A special focus was the further extension of the model to account for inflow turbulence noise. Based on the RANS background flow, synthetic turbulence was modeled and seeded upstream of the propeller blade using the Fast Random-Particle Mesh (FRPM) method and using a specific eddy-relaxation source term for acoustically transparent coupling with the CAA code [7]. The propeller model has been augmented by a Blade Element Theorie (BEMT) model for the propeller blade loads (full-force model based on NLDE and a perturbation force model based on LEE/LNS) utilizing the local flow properties from the LEE/LNS simulations at the blade. The perturbation force approach allowed to compute the response of the blade on inflow turbulence, creating alternating lift forces on the blade.

The simulation of acoustic and vorticity modes was carried out on octree-grids with high-order immersed boundary representation of complex geometries with the DLR code PIANO-IBM. Fig. 18 shows an example computation at the experimental propeller-pylon configuration using the full force model. Results obtained with the simulation chain were reported in Ref. [8].

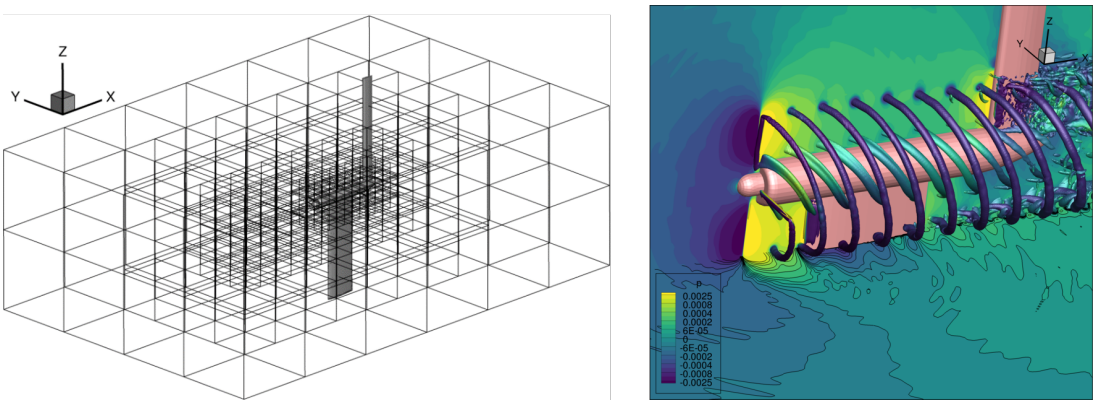


Figure 18: CAA octree-grid of pylon-propeller geometry (left) and acoustic and vorticity field with full-force propeller model (right).

GPUP developed an extension of the Compact Accurately Boundary-Adjusting High-REsolution Technique (CABARET) Wall Modelled LES method to address a wide range of unsteady rotor flow problems. The new algorithm was coupled with the Ffowcs Williams and Hawkings method with averaging over multiple closing control surfaces for far-field noise calculations. The CABARET on rotating grids uses the sliding meshing methodology with maintaining flux conservation at the sliding interface. This was implemented using the so-called super mesh approach, which involves projecting the contact faces located on either side of the sliding interface onto an intermediate virtual surface. The implementation of this technique was centered on the application of sub-cell and sub-face solution reconstructions within hexahedral meshes. The dispersion properties of the CABARET at small Courant–Friedrichs–Lewy (CFL) numbers and non-uniform curvilinear meshes typical of open-rotor applications were further improved. An asynchronous time-stepping algorithm was incorporated resulting in a fast-turnaround time of the solution. The resulting method was implemented on Graphics Processing Units. The CABARET solver on rotating grids was verified on analytical solutions and then validated against the experiment on the A1 and A2 configurations in WP4.1.

RWTH uses the in-house solver framework `m-AIA` on hierarchical Cartesian meshes. In particular, two different noise prediction approaches will be pursued in the upcoming work packages. Both start with a flow simulation within an initial CFD step, employing a pure LES or optionally a combined zonal RANS-LES approach, where only the dominant unsteady noise source region is captured by a LES. The system of equations in the CFD is augmented by porous modeling terms based on the Darcy-Forchheimer model. A cut-cell formulation for the fluid-porous interface is implemented. For the propeller, a level-set-based interface tracking, adaptive mesh refinement (AMR) and dynamic load balancing (DLB) for optimal efficiency and scalability during rotation of the propeller blades are utilized. For moving boundary problems the compressible flow solution is coupled to the Ffowcs-Williams and Hawkings (FW-H) method formulated in the frequency domain to predict the pressure signals at far-field observers. Alternatively, within a two-step CFD-CAA approach, the APE-4 are solved by a higher-order discontinuous Galerkin spectral element method (DGSEM) to predict the wave propagation in the near field. A new porous model, which is derived from the semi-phenomenological Johnson-Champoux-Allard-Lafarge (JCAL) model, was devised.

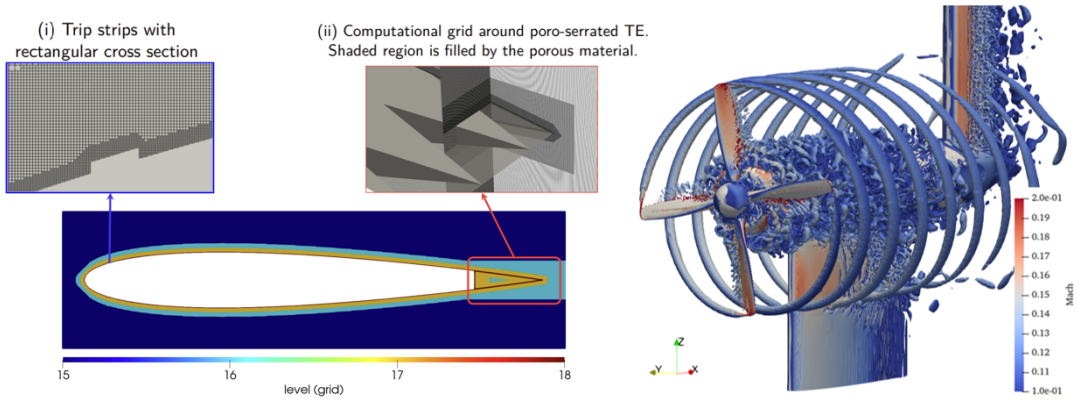


Figure 19: Computational grid of the porous-serrated TE configuration (left) and vorticity field in the BANC-IX propeller-pylon interaction configuration (right).

5.4 Expected contribution in other project work packages

ONERA The ZDES mode 3 + wall model method of ONERA will be applied in WP4 to the simulation of configuration A1, i.e. the interaction between a thick turbulent boundary layer and a propeller considered in the flow conditions matching the UTWE experiments, with the propeller in the static vertical position.

DLR The DLR propeller model will be applied to the wall-mounted and buried propulsion systems (A1 + A2) as experimentally studied by UBRI in WP4.

GPUP The same CABARET WMLES solver coupled with the Ffowcs Williams and Hawkings method will be employed for multidisciplinary optimisation using a multi-fidelity approach for configurations B at baseline and reduced noise designs.

RWTH The aforementioned methodology of RWTH is applied in T2.7. The LES + FH-W approach will be applied in WP4 to the simulation of configuration B1, where three 6-bladed propellers are installed side-by-side on the leading edge of a wing, to investigate the noise generation due to the propeller-pylon interaction in a distributed propulsion system.

5.5 Lessons learnt

ONERA The ZDES mode 3 + wall model method of ONERA is able to resolve the turbulent structures present in the outer layer of the boundary layer, at a much lower cost than the standard ZDES mode 3 approach (i.e. with y+=1 at the wall). A rather long adaptation distance of about 30 times the boundary layer thickness at the inflow is however required when using only the tripping strategy based on the vertical rods.

DLR Successful CAA simulations could be initialized for rather complex imported stl-geometries and a robust workflow could be demonstrated in conjunction with both AD-RANS-based propeller source models as well with perturbation and full-force propeller models.

GPUP Initial results of the CABARET flow and noise solutions for A1 and A2 configurations show an encouraging comparison with the measurements, despite the use of a coarse grid. This suggests that the numerical models have been consistently configured to capture the main boundary layer-rotating blade interaction effects. The good CABARET performance with a coarse LES grid is good news for the multi-fidelity optimization framework, where alternating multiple calls to a fast coarse grid solution with a few calls to a fine grid solution will be used to speed up the convergence.

RWTH For problems with stationary geometries, the two-step hybrid CFD-CAA approach was successfully applied by RWTH during the activities in T2.7. The acoustic porous model in the time domain was observed to be a major improvement in accuracy compared to standard the linearized Darcy-Forchheimer model in terms of dispersion-relation over a large frequency range. For the cases with a rotating propeller, the CFD method has been used to simulate e.g. the BANC-IX propeller-pylon interaction configuration, where a four-bladed propeller is installed upstream of the wing. The flow field results show good agreement with the published experimental data. However, the prediction of the acoustic field cannot easily predicted with the CAA method based on the APE, since no meaningful mean field can be defined. Therefore, a FW-H method has been applied for these cases.

5.6 Deliverables

D2.6 - FRPM/LEE solvers for installed propeller noise - Seyed Mohsen, Alavi Moghadam, Michael Mößner, Roland Ewert (DLR) - 2 November 2021

D2.8 - Extended CABARET and FWH solvers including rotation - Sergey Karabasov, Annabel Markesteijn, Igor Solntsev (GPUP) - 31-08-2021

D2.9 - ZDES solver with wall models - Marc Terracol (ONERA), S. Satcunanathan, M. Meinke (RWTH) - 6 January 2022

5.7 Dissemination

Results obtained with the DLR BEMT model for installed propeller-pylon noise were reported in Ref. [8]. Some details related to the modeling approach are planned to be presented at the upcoming DJINN-ENODISE conference Aeroacoustics Installation Effects in Conventional and New Aircraft Propulsion Systems that will take place November 22-24 2023 at the HdW/bbw in Berlin.

6 Optimization methods (Task 2.5)

6.1 Context and objectives

The objective of the research was to develop optimization methods that can effectively address the installation effects of the noise generated by propellers/open rotors in the context of multi-physics problems,

specifically focusing on aerodynamics and acoustics. The research aims to develop and introduce these methods and to fine-tune these techniques to achieve multi-objective optimization, considering the factors of noise and efficiency.

6.2 Involved partners and work distribution

The work on the development of the optimization method is performed by collaborative efforts of several organizations to address various aspects of the optimization process.

- GPUP (Task leader) aims to contribute by developing a rapid convergence of multi-fidelity optimization approach that utilizes lower-fidelity models and fast turnaround Large Eddy Simulation (LES) numerical simulation accelerated on graphic processing unit (GPUs).
- UR3 focuses on implementation of dynamic adaptive metamodels and dimensionality reduction techniques to reduce the computational efforts required by the optimization processes.
- VKI: VKI's contribution involves adapting their in-house multi-objective optimization platform, CADO, to specifically tackle the challenges posed by multi-copters.
- PVS aims to optimize the distributed electric propulsion (DEP) system using a Reynolds-Averaged Navier-Stokes (RANS) based approach, incorporating VKI's acoustic models through the implementation of the FRONTIER optimization tool.

Through this collaborative effort, the partners bring their expertise and specialized tools to collectively address the objectives of the research, ultimately aiming to achieve improved optimization outcomes in the context of multi-physics and multi-objective optimization.

6.3 Main achievements

GPUP The main achievement of GPUP was the development of a framework based on multi-fidelity design optimization. The framework is applied using a lower-fidelity model to perform most of the optimization runs. The lower-fidelity model is calibrated using a small number of runs on a higher-fidelity model. The two models are the GPU CABARET flow solver coupled with the Ffowcs Williams - Hawkings (FW-H) method for far-field acoustic predictions on a coarse and a fine grid, respectively. Preliminary tests of the framework were performed using analytical and RANS solutions as well as surrogates/metamodels based on data-driven approaches. The metamodels are functions of design parameters, which are iteratively calibrated using higher fidelity solutions within the Multipoint Approximation Method (Figure 20). The effectiveness of the Multipoint Approximation Method (MAM) was verified by conducting benchmark tests that have well-defined optima. The first benchmark problem focuses on optimizing the volume of a Vanderplaats scalable cantilevered beam subjected to a point load. The second benchmark problem involved a multi-physics structural and aerodynamic optimization problem where the objective is to optimize the aerodynamic lift of a wing at a fixed angle of attack and flight altitude. In this benchmark test, an unsteady RANS numerical simulation was coupled with MAM model to continuously provide a feedback loop to the MAM to train the meta-models resulting in the reduced weight and drag for the flight condition under investigation.

PVS The main achievement of PVS is the establishment of the a low-fidelity framework for analyzing distributed electric propulsion (DEP) systems. This framework consists of an open-source parametric geometry engine (OpenVSP), a low-fidelity unsteady three-dimensional panel code (FlightStream), and semi-analytical models for tonal and broadband noise estimation. The framework incorporates an optimization hypervisor (modeFRONTIER) to manage changes in geometric parameters and achieve optimal designs based on desired aerodynamic and acoustic performance metrics. By utilizing low-fidelity and semi-analytical models, this optimization chain can be executed on standard hardware, such as individual workstations, enabling the integration of optimization procedures in early design stages. Figure 21 provides an overview of the framework.

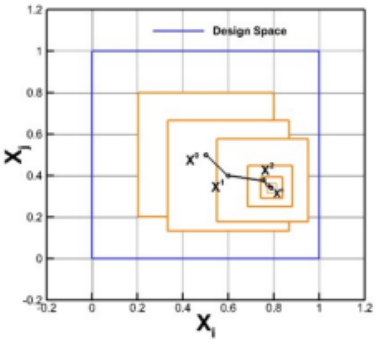


Figure 20: A schematic of the iterative process employed in Multipoint Approximation Method.

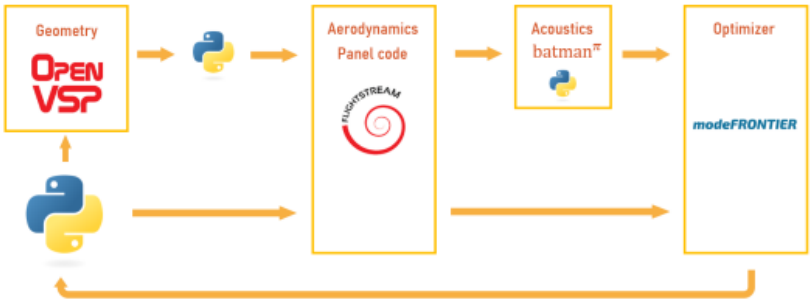


Figure 21: Block diagram of the DEP optimization framework.

VKI The optimization approach utilized by VKI involves the combination of their in-house low-order analytical solver, batmanp, with the modeFRONTIER optimizer developed by pVS. The methodology employs the FlightStream panel method to compute aerodynamic properties such as boundary layer integral parameters (displacement thickness, momentum thickness, skin friction coefficient, and shear stress). These parameters are then used to calculate different sources of noise, including propeller steady loading noise, wake interaction, and wing trailing edge noise, utilizing the Amiet theory. The propeller loading noise is computed using strip theory, while the propagation and farfield acoustic pressure are modeled using Amiet theory in a rotational frame. The resulting farfield noise is fed into the modeFRONTIER optimizer to generate new design parameters, which are then used in FlightStream to obtain updated boundary layer parameters for modified geometry, and batmanp solver to evaluate the noise generated by the modified geometry.

UR3 Two methods were employed by UR3: Adaptive-Stochastic-Radial-Basis-Function-based metamodeling (Adaptive SRBF) and active metamodelling using Artificial Neural Networks (ANN). The Adaptive SRBF-based metamodeling approach is based on the standard (deterministic) RBF (Radial Basis Function) formulation, which involves creating a surrogate model to approximate the relationship between input and output variables in a complex system or process. The RBF was fitted to training data to determine its parameters. Once fitted, the RBF could predict the system's output for new input values. The metamodelling methodology involved an iterative process, as depicted in Figure 4, where the dynamic adaptive metamodel was continuously updated. In active metamodelling using neural networks, a machine learning approach was used to create a predictive model for system or process analysis. This method involves training a neural network using a set of input-output data and subsequently utilizing it to forecast the output for new input data. The developed methodology includes the optimization of the ANN hyperparameters. By leveraging the neural network's predictions of the objective function's output for new input values, the optimization algorithm can concentrate on the most promising regions within

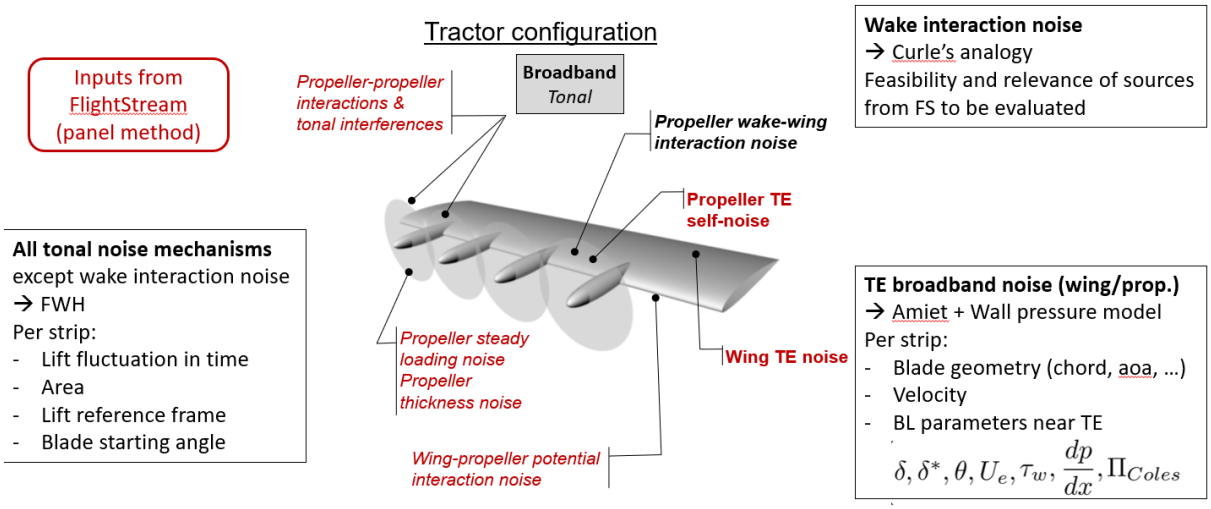


Figure 22: Optimisation methodology.

the design space. The methodology was implemented and tested on the benchmark test case involving subsonic jet interacting with a flat plate.

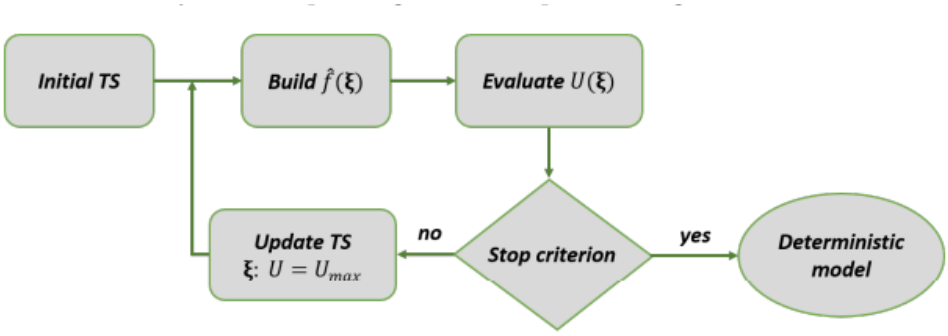


Figure 23: Flowchart of the dynamic adaptive metamodel update.

6.4 Expected contribution in other project work packages

The multi-fidelity approach of GPUP will be applied for aeroacoustics optimization formulation for a multi-rotor configurations of WP5 in puller and pusher configurations (configuration B1/B2). The PVS and VKI will contribute to optimizing the multi-propellers in the puller configuration of WP5 (configuration B1). UR3 will contribute to the optimization/ sensitivity study of the single installed propeller (configuration A1/A2) in WP5.

6.5 Lessons learnt

The installed propeller aeroacoustic design may not have optima in all cases. The optimization process can be improved by re-defining optimization objectives and constraints. Alternatively, the optimization problem may be reformulated as a useful sensitivity study.

6.6 Deliverables

D2.10 - Upgraded optimization methods for DEP and multi-rotors.

6.7 Dissemination

F. Centracchio, S. Meloni, H.K. Jawahar, M. Azarpeyvand, R. Camussi and U. Iemma, Under-expanded jet noise prediction using surrogate models based on artificial neural networks, AIAA 2022-3025.

E. Gallo, A. Zarri, G. Bampanis, M.C. Fasinella and C.F. Schram, Simplified models for propeller potential interaction noise, AIAA 2022-2974.

Meloni S., De Paola E., Centracchio F., Iemma U., Camussi R., "Experimental characterization and data-driven modelling of unsteady wall pressure fields induced by a supersonic jet over a tangential flat plate", Journal of Fluid Mechanics, Vol. 958, A93, 2023.

7 Propulsive efficiency and emissions (Task 2.6)

7.1 Context and objectives

The initial interest behind the BLI and DEP concepts were, in fact, centered around diminishing fuel consumption through the re-acceleration of low-momentum fluid and enhancing lift by generating a flow over the wing. The analysis of the parametric experimental campaign carried out in WP3 delves into aspects such as aero propulsive efficiency and net thrust. The outcomes from both setups will form a comprehensive database, contributing to our understanding of propeller aerodynamic performance while accounting for the impact of installation effects.

7.2 Involved partners and work distribution

- UTWE (Task leader), TUD, UBRI: Apply the Power Balance Method to a tightly integrated propulsion system (config. A)
- UTWE, TUD: Use phase-locked high-resolution stereoscopic PIV as input of the Power Balance Method
- UBRI, TUD, UTWE: Adapt the above method to the employment of porous metamaterials on critical surfaces
- VKI: Aerodynamic performance assessment of multi-rotor (C): torque/RPM/thrust in ALCOVES anechoic room
- VKI, TUD, ONERA: Elaborate a methodology to extrapolate these techniques towards full-scale applications

7.3 Main achievements

UTWE/TUD/UBRI The main achievement of the aforementioned partners was the use of the formulation of the Power Balance Method proposed by Drela [9] in the context of the ENODISE project for Configuration A, using high-resolution stereoscopic PIV as input. In the case of Boundary Layer Ingestion (BLI), the tightly integrated airframe propulsion system results in difficulty to assess the efficiency of the configuration. Due to the coupling of the flow, standard bookkeeping techniques are not reliable and might lead to absurd results. In this context, alternative methods can be used to calculate the propulsive efficiency. Habberman et al [10] showed the possible techniques and their distribution based on the design phase of the aircraft (Figure 24).

The Power Balance Method is ideal if detailed information on the input conditions is known. For the case of ENODISE, where the configurations are defined, and one can determine the inflow conditions through PIV, the PBM is an easy-to-apply method. The performance of the mounted configuration can be assessed, then, with stereoscopic PIV data as input to the PBM. The idea is to use the velocity

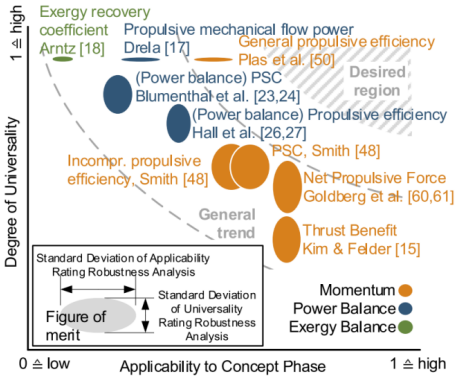


Figure 24: Propulsive efficiency calculation techniques.

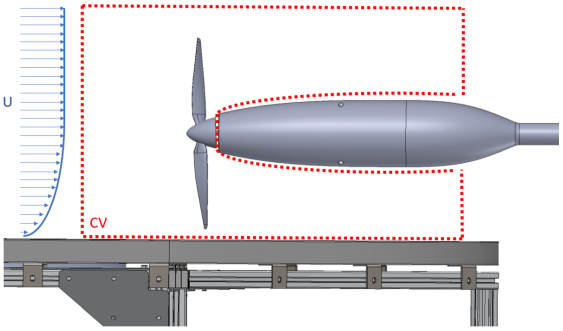


Figure 25: Control Volume of Configuration A.

fields from the PIV upstream and downstream of the propeller disk. Then it is possible to reconstruct the pressure fields using this velocity field [3]. The integral forces and powers are computed using the velocity fields and reconstructed pressures. With those parameters, the PBM technique can be applied. Considering the control volume of Figure 25, the incoming turbulent boundary layer is assessed upstream of the propeller. After calculating the velocity fields and pressure, the integral forces and powers can be assessed along the control volume by scanning many planes in the axial direction. Finally, a modified version of the PBM calculates the thrust, power, dissipation, and deposition energy.

The formulation of the applied PBM for this particular case in the ENODISE project was important to help further setup in terms of expected results and challenges to overcome. It has also shown that, with some level of information, the propulsive benefit can be achieved by only the velocity field, converting it to pressure gradient and further other performance components such as energy dissipation and propeller shaft power.

ONERA considered two examples of aircraft concepts relying on DEP and BLI, with very different approaches to evaluating aeropropulsive performances. The first aircraft (DRAGON, Figure 26) relies on a conventional tube-and-wing architecture implementing an innovative distributed propulsion system. Its design, including aero-propulsive performances, is achieved through a so-called “low fidelity” Overall Aircraft Design software, complemented with additional off-design studies of isolated parameters or disciplines. The second example (NOVA, Figure 27) relies on a disruptive tube-and-wing airframe and an engine implementation in the rear fuselage, taking some benefit of the boundary layer ingestion effect. In this case, all aerodynamic and aero-propulsive characteristics are investigated using a high fidelity CFD (RANS) software and a specific post-process tool to accurately extract all drag components. The tools described in these two examples are not directly available in the ENODISE context. Moreover, their direct application would require a minimal description of an airframe associated to a propulsion system which, again, does not exist with the academic configurations studied in ENODISE.

7.4 Expected contribution in other project work packages

The tools proposed in this task are proposed to all ENODISE partners for an ”a posteriori” evaluation of the aeropropulsive performances of the reference (WP3/WP4) and optimized (WP5/WP6) ENODISE configurations A, B and C, either based on the DEP or on the BLI concepts.

7.5 Lessons learnt

When an engine of any kind interacts with an airframe, any delta between two configurations/regimes must account for this interaction, which requires a minimum of information on the airframe flow, for example the velocity profile (or thickness) of the boundary layer in which the propulsion system is partly



Figure 26: DRAGON aircraft concept.

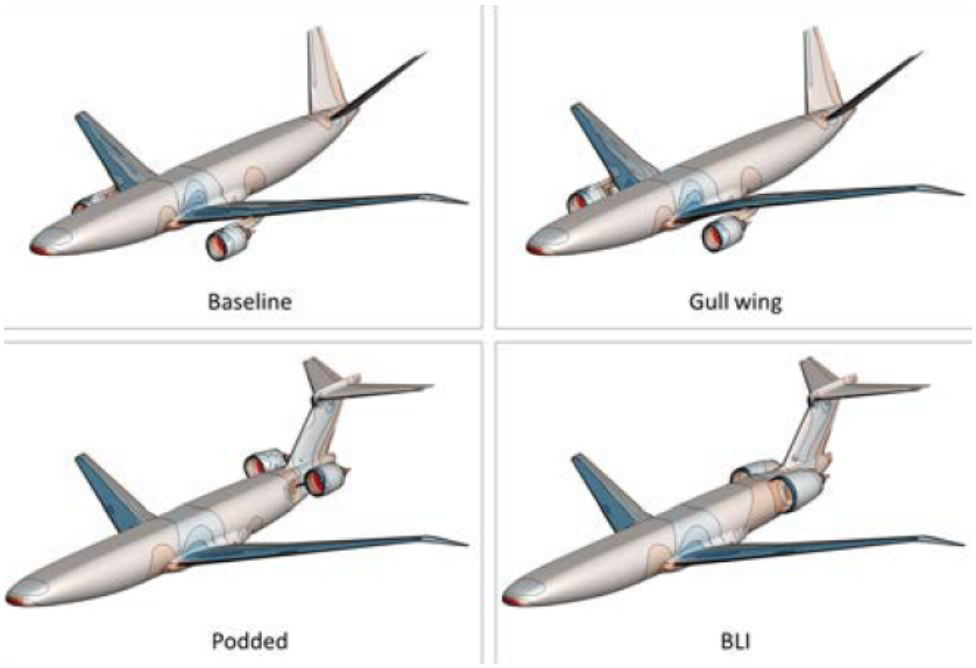


Figure 27: NOVA aircraft concepts.

immersed. In this situation, which is actually the case of most ENODISE academic configurations, since the project objective is precisely to study the airframe/engine interactions, one should rely on the Power Balance Method.

7.6 Deliverables

D2.11 - Power Balance Method for the experimental characterization of the aero-propulsive efficiency of tightly-integrated propulsion systems - L.D. de Santana (UTWE), L. Castelucci (UTWE), D. Ragni (TUD), F.N. Monteiro (TUD), Georgios Bampanis (VKI) - November 17, 2021.
D2.12 - Model relating aero efficiency w/pollutant emissions - ´Eric Manoha (ONERA) - 28 February 2022.

8 Porous materials and advanced liners (Task 2.7)

8.1 Context and objectives

To measure/model porous materials for the mitigation of the adverse effects associated with the tighter integration of propulsive systems.

8.2 Involved partners and work distribution

- TUD (Task leader), UBRI, UTWE: Design, 3D-print, characterize porous samples mathematically-defined (porosity, permeability)
- VKI: Turbulent gust/BL interacting with partially porous NACA airfoil : 1/ Experiment and physical analysis in JAFAR
- RWTH: 2/ Prediction of noise mitigation with porous material with fully coupled CFD/CAA and porous model
- UBRI, UTWE: Test porous treatments and liners placed before/along the S-Shaped to reduce acoustic reflections

8.3 Main achievements

TUD A synthetic unit-cell geometry has been proposed to be designed and manufactured into porous TE/LE/or fairing inserts, which can be adopted and later manufactured for a direct comparison with simulation results. The porous material proposed in the present study has a unit-cell geometry that is based on the diamond lattice structure. The unit cell consists of a network of cylindrical struts. The unit-cell dimension is scaled to D = 6.36 mm, such that the resulting porous insert produces comparable noise reduction level and spectral features as those of the metal-foam insert previously tested in Rubio Carpio et al. [11]. The aerofoil span, drawing and dimensions are shown in Figure 28.

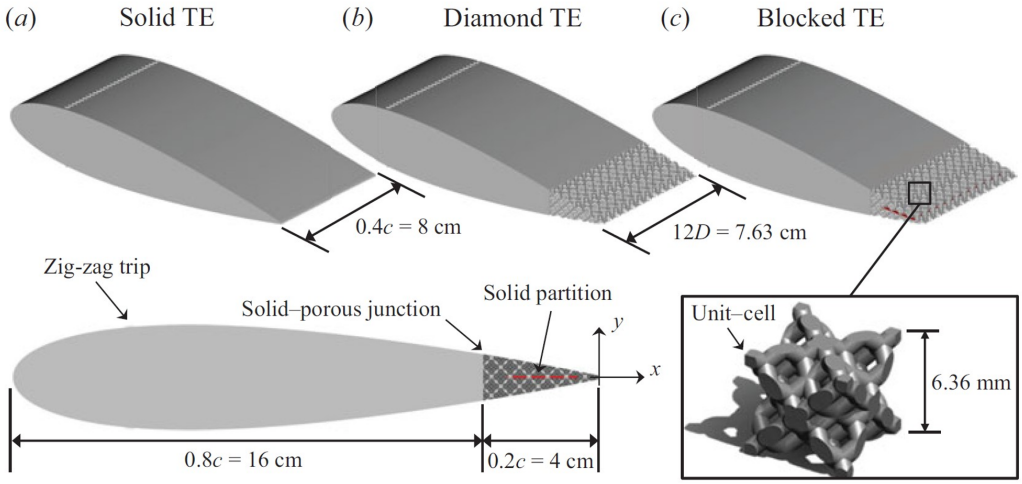


Figure 28: 3d printed diamond open-cell, study from Teruna et al. [12]: a drawing of the NACA 0018 with solid (a), porous (b) and blocked (c) TE configurations. A lateral view of the aerofoil with blocked TE is shown at bottom left, besides which is an inset depicting the unit-cell geometry.

In the full study from Teruna et al. [12] it is demonstrated that the diamond-cell material achieves a substantial noise reduction at low frequencies, although a slight noise increase is found at high frequencies. The study additionally shows how to relate the material properties to the flow parameters,

by the employment of the entrance length associated with the porous material geometry. The velocimetry data showed that the permeable surface created an increase in boundary-layer thickness on the pylon's suction side. This resulted in a loss of lift and an increase in local drag, but effectively reducing the velocity fluctuations near the pylon's surface up to 35%. Microphone array measurements showed that this led to a minor reduction in the far field noise (¡1 dB). More pronounced reductions in far-field noise were obtained for inserts with larger cavity depth but resulted in larger aerodynamic performance losses. Details of the study can be read in:

Sinnige, T., Corte, B. D., De Vries, R., Avallone, F., Merino-Martínez, R., Ragni, D., ... & Veldhuis, L. L. (2019). Alleviation of propeller-slipstream-induced unsteady pylon loading by a flow-permeable leading edge. Journal of Aircraft, 56(3), 1214-1230.

UBRI Characterisation of porous iron foam structure to evaluate porosity and permeability. Porosity of the iron foam samples were characterized using Computed Tomographic (CT) scanning, while permeability was tested using a custom permeability test rig. The porosity study was carried out using a Nikon XT H 320 LC computed tomography scanner. A number of X-ray radiographs projection images were taken at different projection angles through the porous sample, as seen on a detector. The X-ray beam energy attenuation relies upon the density and the thickness of the porous sample in the direction of the beam and the attenuation behaves exponentially in nature in relative to the thickness of the porous sample. The porous sample in this Task was the 35PPI sample, which the CT results show a porosity value of $\phi = 88\%$. Permeability was tested in the setup depicted in Figure 29. The pressure drop across a cylindrical test sample was measured, and the airflow permeability was calculated using the Dupuit-Forchheimer equation. Pressure ports were drilled into the side of the tube to allow pressure measurements. This analysis yielded a permeability value of $4.4166x10^{-8}$ m^2 for the tested 35PPI sample. This grade of porous media was then supplied to UTWE for A1 testing.

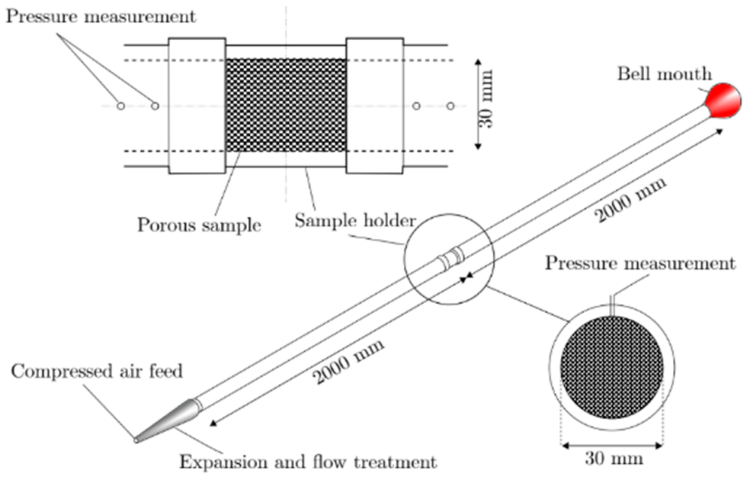


Figure 29: Permeability test rig

UWTE For Configuration A1 at the UTWE wind tunnel, two absorption surfaces were tested and compared with the baseline flat plate. The first surface is a collection of mitigation units of 3D-printed blocks with small tubes in it. Each one of the tubes acts as a quarter-wavelength resonator. Those tubes were designed using the "Low reduced frequency model" and are more efficient than liners due to the porosity one can achieve in relation to the size of the sample. Those quarter-wavelength resonators were designed to absorb noise at the mid-range frequency (between 800 Hz and 1500 Hz), where the absorption coefficient was higher than 90%. Those units are distributed underneath the propeller, on a one-diameter square area, with the concern of covering the regions where the blade is passing close to

the plate, to avoid resonant effects with the units. The second surface was a porous metal with 35 ppi and 88% porosity. The comparison between the two materials and the baseline can be seen in Figure xx (2 Bladed Maijzlik propeller – 12"x18", 6000 RPM, J = 0.98).

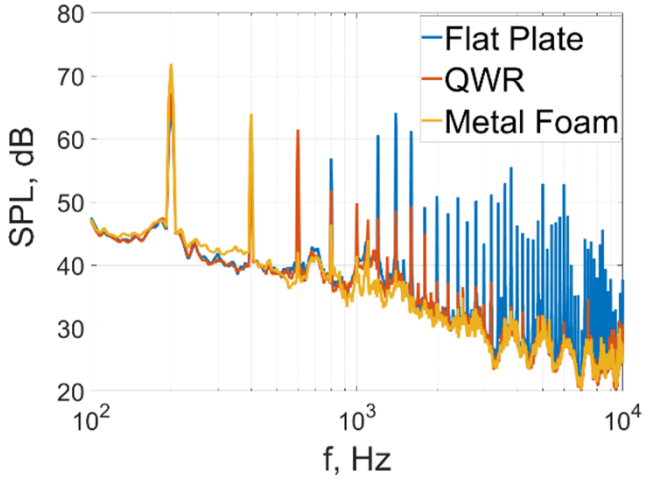


Figure 30: Acoustic spectra for the A1 configuration with resonators and porous media mitigation techniques

Although the quarter-wave resonator is designed specifically for a certain frequency range of absorption, the metal foam was more efficient in absorbing noise at that region. Only on the lower frequency range, there is a small increase in broadband noise, but overall the foam is efficient for the tonal noise reduction from the 3BPF on.

RWTH In T2.7 RWTH performed simulations of NACA airfoils with porous surface treatments to investigate leading and trailing edge interactions of gusts and turbulent boundary layers. Details about the methodology and an investigation of leading-edge turbulence impingement noise on a rod-airfoil configuration were issued in deliverable D2.13. Furthermore turbulent boundary layer trailing-edge noise mitigation by porous surface treatments for flows at $M_\infty = 0.1118$ and $Re_c = 1 \times 10^6$ around two NACA 0012 airfoils at α=0° and α=4° have been investigated. A baseline configuration corresponding to a classical NACA airfoil with a solid sharp trailing-edge was compared against an airfoil with a poro-serrated trailing-edge, extending over the last 15 %, where the serrations are filled by a porous material.

The geometric inhomogeneity of the poro-serrated causes the flow field, and hence the turbulent statistics to vary in the spanwise direction. The analysis revealed that the porous treatment at the current flow conditions has only a local effect on the one-point statistics, i.e., the flow encountered over the solid part of the serrations resembles the flow over a pure solid TE. The evaluation of the aerodynamic performance revealed a reduction of the lift-to-drag ratio by 29%, mainly driven by a substantial increase in drag, which is primarily caused by the contribution of Reynolds shear stress to the overall shear stress acting on the porous surface. Acoustic predictions for $\alpha = 0°$ and $\alpha = 4°$ are qualitatively similar. The most important finding is that the poro-serrated airfoil shows a significant low-frequency noise reduction for all observer angles compared to the baseline. However, towards higher frequencies the tendencies are reversed and the poro-serrated airfoil shows significantly higher levels especially in the sideline and downstream directions. It is interesting to note that the present modeling does not include any surface roughness effects, which is often attributed for the excess noise at higher frequencies observed in experiments, but still predicts a high frequency noise increase for the present poro-serrated TE. To conclude, these findings suggest, that despite the increased turbulence intensity level over a porous surface predicted by the CFD, a noise mitigation in certain frequency ranges can be achieved. The respective noise directivities are published in [13]. To understand the noise sources the flow field was analyzed with respect to flow profiles of mean and fluctuating quantities, e.g. the turbulent kinetic energy, one-point

wall pressure spectra, spatial coherence of wall pressure fluctuations and length scales derived thereof. Results obtained for the coherence of the baseline and the tip plane of the poro-serrated airfoil exhibit strong similarities, whereas the length scale derived from the coherence shows a considerable reduction at low frequencies over the root of the serrations. These findings suggest that the elongated streaky structures aligned in the streamwise direction, commonly observed in regular turbulent boundary layers over solid surfaces, may be weakening in this particular setup. These observations align with the noise reduction seen in the CAA.

VKI Within the context of Task 2.7, VKI has investigated the impact of integrating a porous material into the structure of an airfoil subjected to incident turbulence on the surface-pressure fluctuations. The purpose of this activity has been to elucidate the physical noise-reduction mechanisms of this technology to provide valuable insight into the design of innovative and efficient passive strategies that can be used in WP5. The results from large-eddy simulations, which were previously validated with measurements conducted in the JAFAR facility, show that the porous treatment of the airfoil yields an attenuation of the unsteady-pressure peak, which is localized in the low-frequency range of the spectrum and is induced by the milder distortion of the incoming vortices. However, porosity is ineffective in breaking the spanwise coherence or in-phase behaviour of the surface-pressure fluctuations. Furthermore, an additional dipolar source term associated with the non-zero unsteady Reynolds stresses on the porous surface is found to be considerable in the stagnation region of the airfoil, where the transpiration velocity is larger. This term is partly correlated with the unsteady surface pressures, suggesting constructive interference between the two sources that results in a non-negligible contribution to the radiated far-field acoustic pressure for observation angles near the stagnation streamline.

8.4 Expected contribution in other project work packages

All techniques presented in this section could be used for mitigation strategies, as defined in WP 6 - Mitigation of adverse installation effects.

The 35PPI porous media is to be installed and tested in configuration A1 by UTWE as part of WP6 experimental campaign to further assess the effect on acoustic reflections.

8.5 Lessons learnt

TUD Results from the work at TU Delft have shown that materials with a repeatable and uniform (or at least periodic) permeability sensor can be leveraged to produce a reduction of the pressure fluctuations at the edge with a considerable decrease of radiated noise. To achieve optimal aerodynamic performance, the entrance length of the material needs to be tuned with respect to the boundary layer characteristics or with the incoming turbulence scales.

VKI The guidelines that can be extracted from the VKI's analysis indicate that the porous treatment should be confined to a region just downstream of the leading edge, where the unsteady surface pressures are maximum. This is expected to limit the aerodynamic performance loss typically linked to this passive noise-mitigation strategy that leads to a decrease in lift and an increase in drag. Furthermore, a spanwise-varying distribution of pores could help break the spanwise coherence or the in-phase behaviour of the surface-pressure fluctuations through a mechanism similar to that induced by leading-edge serrations. Finally, preventing the flow from permeating the leading edge could counteract the noise contribution due to the non-zero Reynolds stresses on the porous surface and the possible deterioration in lift force associated with it.

UTWE From the study carried out at UTWE, the porous media outperformed the quarter-wave-resonators in the frequency region the resonators were tuned for, but experienced a mild uplift in the low-frequency broadband. The use of porous media proves to be very effective in reducing tonal harmonics.

UBRI CT and permeability rig are effective at characterising porous media in terms of both porosity and permeability.

RWTH The most important finding is that the poro-serrated airfoil shows a significant low-frequency noise reduction for all observer angles compared to the baseline. However, towards higher frequencies, the tendencies are reversed and the poro-serrated airfoil shows significantly higher levels, especially in the sideline and downstream directions.

8.6 Deliverables

D2.13 - Low-order and high-order models for porous materials - S. Satcunanathan, M. Gondrum, and M. Meinke (RWTH) R. Zamponi, C. Schram (VKI) - 26 August 2022

D2.14 - New porous materials for minimal aerodynamic penalty - Daniele Ragni, Hasse Dekker (TUD) - 31 July 2022

8.7 Dissemination

RWTH - publication of numerical model [13].

UBRI - publication of porous media characterisation [14].

9 Leading edge / trailing edge serrations (Task 2.8)

9.1 Context and objectives

This part of the project is aimed at developing and designing methodologies to assess the potential of leading-edge (LE) and/or trailing-edge (TE) serrations on propeller blades for noise reduction in BLI and DEP systems. Best-practice rules for the dimensions of serrations and their compatibility with manufacturing constraints are key aspects.

9.2 Involved partners and work distribution

- ECL (Task Leader): assessment of LE serrations to reduce inflow-turbulence noise and to delay dynamic stall on the blade; bibliographical survey, dimensional analysis and dedicated experiments on small rotors
- VKI: assessment of TE serrations to enhance wake mixing and reduce trailing-edge noise, and noise due to wake interaction with downstream elements; dedicated experiments on isolated airfoils

9.3 Main achievements

ECL A bibliographical survey and a dimensional analysis of the effects of leading-edge and trailing-edge serrations were made by ECL. The devices are aimed at reducing broadband noise from turbulence-edge interactions, independently of aerodynamic efficiency, but they often cause degraded aerodynamic performances. Simple experiments performed with small-size drone rotors also show that significant broadband-noise reductions were achieved with add-on small-size serrations at the leading edge in undisturbed flow. The suspected action, maybe typical of low-Reynolds number flow regimes, was the reduction of a leading-edge separation bubble. Typical reductions in a wind-tunnel experiment with a 3-bladed Mejzlik rotor of 20 m diameter in a jet of 30 cm diameter are illustrated in Fig. 31. Only the blade tips operate in disturbed flow.

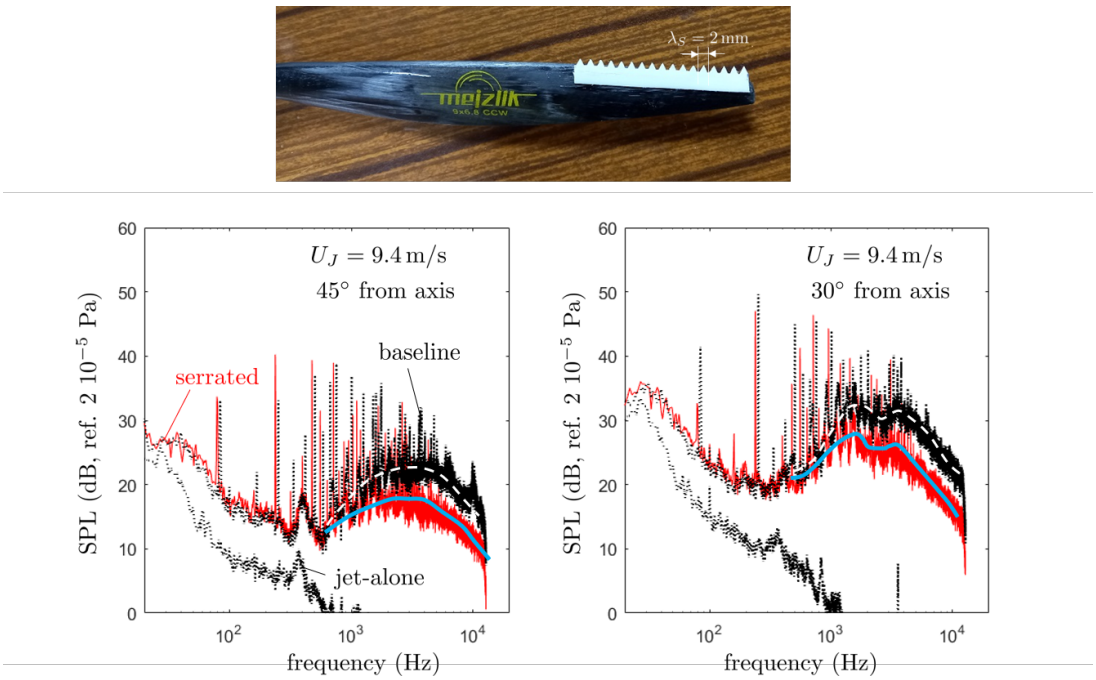


Figure 31: Measured sound spectra for a 3-bladed propeller in the core of a round jet, condition of blade-tip turbulence interaction. ECL experiment. Top: view of the added serrations. Advance ratio 0.54, tip Mach number 0.17.

VKI Experiments made at VKI established general trends for trailing-edge serrations on the NACA-65(12)-10 airfoil. Trailing-edge noise is reduced at moderate/middle frequencies, whereas sound is regenerated at high frequencies, with details depending on serration shape, flow speed and angle of attack. Dedicated PIV measurements confirmed that the cross-flow between serration teeth is responsible for the regeneration. Mixing is also accelerated in the wake, suggesting that the wake-impingement noise on downstream bodies should be reduced. Typical serration shape and noise-reduction spectra are shown in Fig. 32.

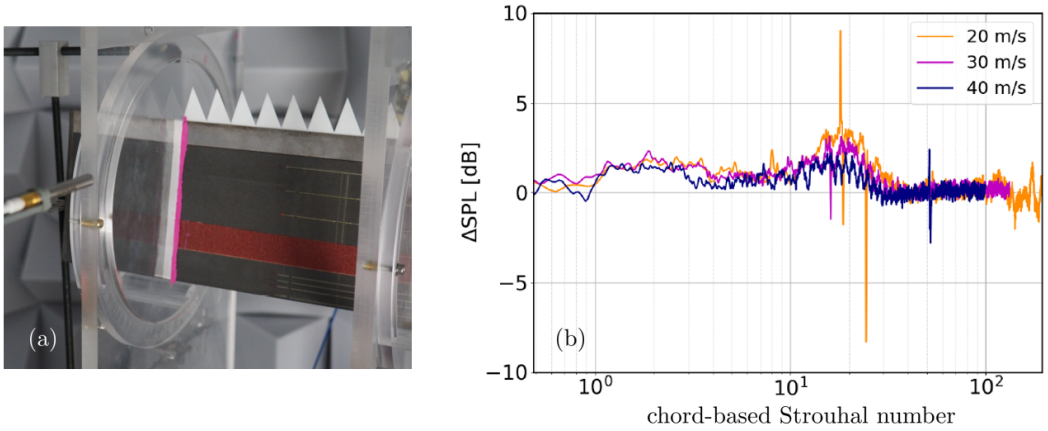


Figure 32: (a): detail of the experimental setup at VKI. (b): typical noise-reduction spectra (positive values correspond to reduction), at −5° angle of attack.

9.4 Expected contribution in other project work packages

Basic outcomes will be used as guidelines for noise mitigation tests by other partners.

9.5 Lessons learnt

In both cases, serration wavelengths must be tuned to the scales of the incriminated turbulence for optimum broadband-noise reduction. The effect of leading-edge serrations is Reynolds-number dependent. It could be also aerodynamically beneficial for sub-critical flow regimes on blades, irrespective of the presence of inflow disturbances. Sound regeneration at high frequencies for trailing-edge serrations is inherent to the cross-flow caused by loading. It could be mitigated by flexible, adaptive add-ons.

9.6 Deliverables

D2.15 – Leading edge / trailing edge serrations for reduced turbulence-impingement noise and trailing edge noise - Daniel Acevedo (ECL), Erica Gallo (VKI), Michel Roger (ECL) - 19 September 2022

10 Conclusions on WP2

In ENODISE, WP2 has an atypical and transverse position with respect to the four "pillars" work-packages (Experiments, Simulations, Optimization, Mïtigation) and thus can be seen as a toolbox for the whole project, gathering methodologies and technologies already existing in the partners' background but requiring consolidation considering the specific challenges raised by the complex physical mechanisms and specific objectives of ENODISE. So, this toolbox can be seen as a collection of about 24 independant bricks or activities, covering a large spectrum and aspects of the research on the noise generated by rotating machinary. Indeed, the collection of the 15 technical reports generated by the involved partners might be issued as a single encyclopedic volume that could be of great help for researchers in this field. The drawback of this diversity is that drawing global conclusions from the whole workpackage is not straightforward, even if a a clear commonality between all activities is the need to improve existing methodologies to adapt them, firstly to the specific academic DEP and BLI configurations studied in WP3/4/5/6, but also to the extrapolation to full-scale real-world configurations in WP7. Beyond the difficulty to draw global conclusions, in each task section of the present report, the reader will find what lessons have been learnt throughout the activities of WP2, and how the improved methodologies and technologies will be used in other workpackages.

References

[1] D. Ragni, B. W. Van Oudheusden, and F. Scarano. 3D pressure imaging of an aircraft propeller blade-tip flow by phase-locked stereoscopic PIV. *Experiments in Fluids*, 52(2):463–477, 2012.

[2] D. Schanz, S. Gesemann, and A. Schröder. Shake-the-box: Lagrangian particle tracking at high particle image densities. *Experiments in Fluids*, 57(5):1–27, 2016.

[3] J.F.G. Schneiders and F. Scarano. Dense velocity reconstruction from tomographic ptv with material derivatives. *Experiments in Fluids*, 57(9):1–22, 2016.

[4] R. Pieren L. Bertsch S. A. Rizzi, I. LeGriffon. A comparison of aircraft flyover auralizations by the aircraft noise simulation working group. *AIAA Paper 2020-2582, AIAA AVIATION 2020 FORUM, June 15-19, 2020.*

[5] R. H. Thomas I. LeGriffon J. C. June I. A. Clark M. Lorteau L. Bertsch, L. Sanders. Comparative assessment of aircraft system noise simulation tools. *Journal of Aircraft*, 58(4), 2021.

[6] L. Sanders I. LeGriffon. Aircraft noise impact assessment at onera. *DLRK Deutscher Luft und Raumfahrt Kongress, virtual*, 2020.

[7] Varun Bharadwaj Ananthan, Juergen Dierke, Roland Ewert, and Johannes Kreuzinger. Wall-modelled les on hierarchical cartesian mesh for trailing edge noise prediction. In *28th AIAA/CEAS Aeroacoustics 2022 Conference*, 2022.

[8] Seyed Mohsen Alavi Moghadam, Juergen Dierke, Michael Moessner, Roland Ewert, and Jan Delfs. A mid-to-high fidelity aerodynamic noise simulation framework for installed propeller configurations. In *28th AIAA/CEAS Aeroacoustics 2022 Conference*, 2022.

[9] Mark Drela. Power balance in aerodynamic flows. *AIAA journal*, 47(7):1761–1771, 2009.

[10] AL Habermann, J Bijewitz, A Seitz, and M Hornung. Performance bookkeeping for aircraft configurations with fuselage wake-filling propulsion integration. *CEAS Aeronautical Journal*, 11(2):529–551, 2020.

[11] A. Rubio Carpio, F. Avallone, D. Ragni, M. Snellen, and S. van der Zwaag. Mechanisms of broadband noise generation on metal foam edges. *Phys. Fluids*, 31, 10, 2019.

[12] C. Teruna, F. Avallone, D. Ragni, A. Rubio-Carpio, and D. Casalino. Numerical analysis of a 3-d printed porous trailing edge for broadband noise reduction. *J. Fluid Mech.*, 926, A17, 2021.

[13] Sutharsan Satcunanathan, Matthias Meinke, and Wolfgang Schröder. Numerical analysis of poro-serrated trailing-edge noise. In *AIAA 2022-2817*, 2022.

[14] Showkat Ali and Syamir Alihan. *Flow Over and Past Porous Surfaces.* PhD thesis, University of Bristol, 2018.